PERGAMON

International Journal of Heat and Mass Transfer 42 (1999) 1747–1755

International Journal of HEAT and MASS TRANSFER

EHD-assisted external condensation of R-134a on smooth horizontal and vertical tubes

K. Cheung, M.M. Ohadi*, S.V. Dessiatoun

Heat and Mass Transfer Enhancement Laboratory, Department of Mechanical Engineering, University of Maryland, College Park, MD 20742, U.S.A.

Received 22 May 1997; in final form 25 August 1998

Abstract

In this paper, results of an experimental study on the EHD-assisted external condensation of R-134 over a plain tube will be presented and discussed. The experiments performed can be divided into two groups: (1) EHD-assisted external condensation on a vertical smooth tube and (2) EHD-assisted external condensation experiments on a horizontal smooth tube. In each case, experiments were conducted as a function of parametric values such as heat flux, electrode gaps and applied electric field potential. All of the experiments were conducted using a specially designed helical electrode and with R-134a as the working fluid.

Experimental results demonstrate a remarkable potential in utilizing EHD to enhance external condensation heat transfer. It is concluded that the enhancement is driven by the effective removal of the condensate through EHD-induced liquid extraction and dispersion phenomena. © 1998 Elsevier Science Ltd. All rights reserved.

Nomenclature

A heat transfer surface area
c_p specific heat
D diameter
g gravity
h averaged heat transfer coefficient (based on averaged temperatures)
h_{fg} latent heat of evaporation
I heater current
I_e applied EHD current
k thermal conductivity
L test section length
P pressure
Q heat transfer rate
q heat flux
T temperature
V heater voltage.

Greek symbols

α EHD power consumption ratio
Γ mass flow rate
η enhancement factor
ϕ applied EHD voltage.

Subscripts

0 base case
EHD electrohydrodynamic
l liquid
max maximum
opt optimum
sat saturation
v vapor
w wall.

1. Introduction

Utilization of electric field to enhance external condensation heat transfer has benefited from significant progress in recent years. According to works by Didkovsky and Bologa [1], Yabe et al. [2], Sunada et al. [3] and Yamashita and Yabe [4], condensation heat transfer was significantly improved by EHD for a variety of working fluids such as R-113, R-123 and other organic substances. A prototype EHD condenser was successfully built and

* Corresponding author. Tel.: 001 301 405 5263; fax: 001 301 405 2025; e-mail: ohadi@eng.umd.edu

0017–9310/98/$ - see front matter © 1998 Elsevier Science Ltd. All rights reserved
PII: S0017–9310(98)00291–9

tested by Yamashita et al. [5]. Their experimental results further demonstrate the feasibility of implementing EHD technique in a practical heat exchanger. With the concern of ozone depletion, R-134a is considered to be an environmentally friendly alternative to the commonly used R-12. However, none of the previous works tested R-134a for external condensation with electric field. The objectives of the present experiments were (1) to identify the potential of EHD heat transfer enhancement technique on external condensation with R-134a in both vertical and horizontal tube orientations, (2) to gain a better understanding of the heat transfer enhancement mechanism and (3) to quantify the effects of the parameters of interest on EHD-assisted external condensation.

2. Experimental apparatus and procedure

2.1. Experimental apparatus

A new experimental setup was carefully fabricated to conduct external condensation experiments under the EHD effect. The setup had several main design features: it was capable of conducting experiments for external condensation in both vertical and horizontal orientations, it enabled the performance of flow visualization studies and it was equipped with computerized control systems. The schematic diagram of the setup is shown in Fig. 1. The major components included the test section, the condensation chamber, the computerized environmental chamber temperature-control unit and the computerized condensation chamber pressure-control unit.

2.1.1. Environmental chamber temperature control unit

As shown in Fig. 1, the condensation chamber was housed in an enclosed space (environmental chamber) where its temperature was regulated by an environmental temperature control unit. The control unit consisted of a R-12 refrigeration loop, a resistive heater and a computer interfaced feedback system, so that it was capable of providing cooling or heating depending on demand. Thermocouples were placed inside the enclosed space to record the average environmental chamber temperature. Based on readings of thermocouples, the computer sent on/off control signals to the refrigeration unit and the heater. Typically, the system could monitor the environmental chamber temperature within ± 0.4 K.

2.1.2. Condensation chamber

The main body of the condensation chamber is shown in Fig. 2. It consisted of a cylinder shell and two aluminum square flanges. The cylinder shell was made of tempered glass, which could sustain up to 689.5 kPa (100 psia) in pressure. It had an inside diameter of 127 mm (5.00″) and a wall thickness of 9 mm (0.35″). The flanges were tightened against the cylinder shell by four stainless steel rods, each having a diameter of 19 mm (0.75″) and a length of 381 mm (15″). Both the upper and lower flanges had dimensions of $178 \times 178 \times 51$ mm ($7'' \times 7'' \times 2''$). Gaskets made of Teflon were placed in the junctions between the flanges and the edges of the glass cylinder to prevent refrigerant leakage. The inside surfaces of the flanges were covered with 7.0 mm (0.28″) thick plastic sheets, giving additional thermal resistance to heat transfer.

Two access valves were installed on the condensation chamber, one on the upper and the other on the lower flange. They were mainly used for refrigerant charging and discharging purposes. Also mounted on the flanges were the cartridge heater, the applied EHD voltage connection and the measurement devices, including the pressure transducer and the probe for saturation temperature measurement. Refrigerant vapor was generated from the cartridge heater that was submerged in the liquid pool as shown in Fig. 2. The amount of heat input from the heater was controlled by a variable transformer. As a safety precaution, the condensation chamber was equipped with a relief valve and a pressure switch. If the chamber pressure were to approach its design limit, the relief valve would open and the power to the heater would be switched off automatically.

2.1.3. The test section

In this experiment, a smooth tube with a nominal diameter of 19 mm (0.75″) and a length of 200 mm (7.9″) was used. As shown in Fig. 3, 9 thermocouples (T-type) were mounted on the inside wall of each tube for wall temperature measurement. They were placed at 3 axial locations at 51 (2.0″), 102 (4.0″) and 154 mm (6.0″) along the test section tube. At each axial location, as depicted in Fig. 3, three thermocouples were evenly distributed, 120° apart from each other. Heat removal from the test section was done with chilled water from a separate water chiller. An annular water passage was used in the test section tube to provide more uniform cooling for the test section.

2.1.4. The electrode

In the present work, a specially designed helical electrode was developed for EHD-assisted external condensation. The new electrode implements a continuous, multi-step helical-mesh structure which combines the advantages of conventional mesh and helical electrodes. In addition, the electrode is installed with promoters, which help in initiating the extraction of liquid condensate. Details of the electrode structure can be found in Cheung [6].

2.1.5. Pressure control system

The pressure inside the condensation chamber was maintained by removing a precise amount of heat from the condensing tube. This was achieved by sim-

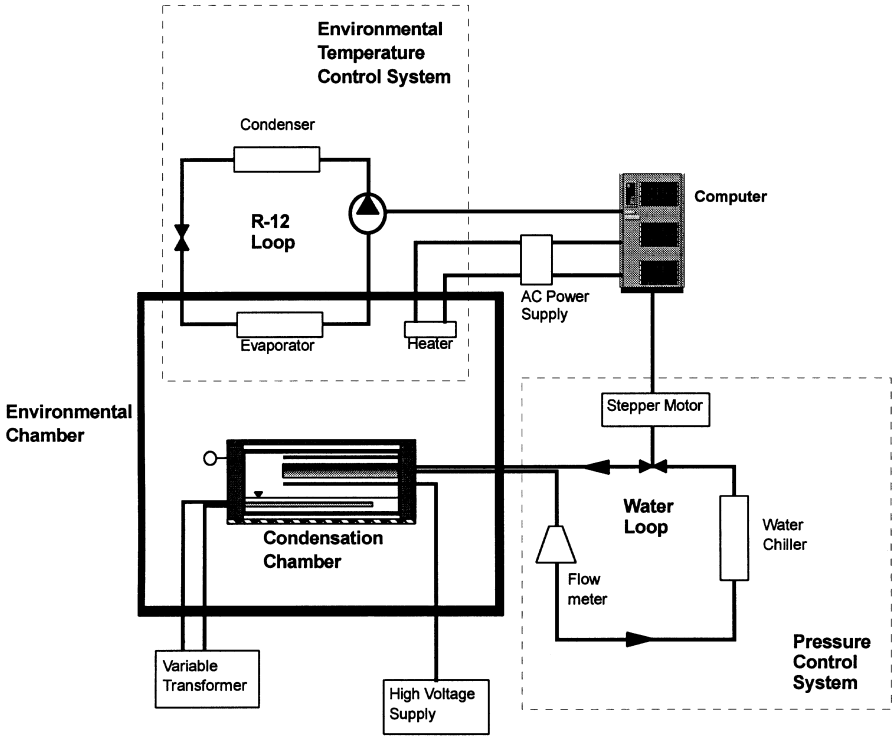

Fig. 1. Schematic of the external condensation experimental setup.

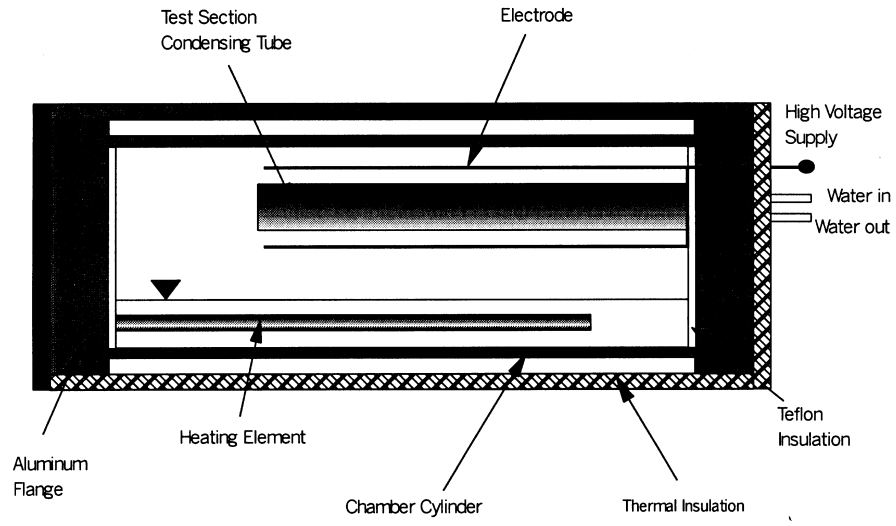

Fig. 2. Details of the condensation chamber.

ultaneously regulating the water flow rate and correcting the water temperature. Water was chilled in a separate chiller with 1.5 kW cooling capacity and circulated in a closed loop manner by a water pump. Two thermocouples were submerged in the water pool to measure the water temperature and the computer continuously checked the temperature. Utilizing the feedback loop with on/off signals to the chiller, the unit maintained deviations of water temperature from the preset value within ± 0.2 K. In addition, a regulating valve, assisted

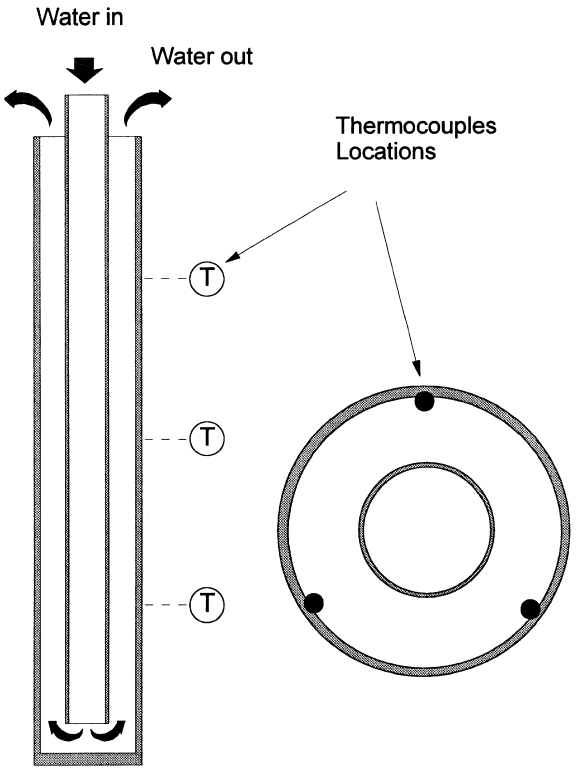

Fig. 3. Locations of the thermocouples.

by a stepper motor and a computerized control device was installed in the water loop, providing automated flow rate adjustment. Measurement of system pressure was provided by a pressure transducer, which had a working range of 0–689.5 kPa (0–100 psia). The chamber pressure control unit kept the saturation pressure in the chamber within ± 0.345 kPa (± 0.05 psi) of the pre-determined value.

2.2. Test conditions for the EHD-assisted condensation experiments

All of the EHD-assisted condensation experimental data were collected using R-134a. The saturation pressure was maintained at 551.6 kPa (80 psi), which corresponds to a saturation temperature of 18.8°C. The SEC-001 electrode was used for all experiments, testing with different three electrode gaps. For convenience, other parametric test ranges are summarized in Table 1.

2.3. Experimental procedure

As in a typical condensation experiment, the condensation heat removal rate was fixed, and data were taken at various EHD applied potentials, ranging from the maximum allowable level down to zero. The experimental procedure began by switching on the water chiller and the water pump. Then, the power of the heater was set according to the pre-determined condensation heat rate. Next, the high voltage supplier was turned on and the voltage potential was adjusted to the highest level to be tested for the given experimental run.

Table 1
Test conditions for the smooth tube condensation experiments

Parameters	Ranges
Working fluid	R-134a
Saturation pressure (P_{sat})	551.6 kPa
Electrode gap (δ_e)	0.8, 1.6 and 3.2 mm
Heat flux (q)	2600–49 000 W m^{-2}
Applied voltage (ϕ)	0–26 kV

The pressure of the condensation chamber was controlled through the adjustment of water flow rate and the water temperature entering the condensing tube. In order to obtain a more uniform test section wall temperature, it is preferable to have a higher water flow rate, which gives a smaller temperature difference between the inlet and outlet water temperature of the condensing tube. Preliminary adjustments were done until the pressure of the chamber stabilized to within ± 1.38 kPa (± 0.2 psi) of the pre-determined value. From then on, the computer took over and monitored the chamber pressure by adjusting the water flow rate. From previous experience, it was known that the computerized control device was capable of maintaining a pressure tolerance within ± 0.345 kPa (± 0.05 psi). In general, it took about 4 h for the system to reach steady state condition, where the fluctuations of saturation pressure, temperature, and EHD current were less than $\pm 1\%$ for a sample period of approximately 5 min. Once the system became steady, data were taken for the wall temperatures at the nine locations, the vapor temperatures and the EHD current. Then, the applied EHD voltage was set to the next level and the above procedure was repeated.

3. Data reduction

In a closed system, the heat removed from the test section tube is equal to the heat input from the electrical heater when the boundary of the chamber is considered adiabatic. Therefore, with that assumption the condensation heat removal rate can be calculated as

$$Q = VI \tag{1}$$

where V and I are the heater voltage and current, respectively. The heat transfer surface area of the tube is determined by

$$A = \pi DL \tag{2}$$

The wall temperature (T_w) is taken as an average of nine thermocouples measurement

$$T_w = \frac{\sum_{i=1}^{9} T_i}{9}. \quad (3)$$

Similarly, the saturation temperature in the condensation chamber (T_s) is evaluated as an average of the three temperature readings:

$$T_s = \frac{\sum_{i=1}^{3} T_i}{3}. \quad (4)$$

Consequently, the EHD-enhanced condensation heat transfer coefficient (h) averaged over the test section length is defined as

$$h = \frac{Q}{A(T_s - T_w)}. \quad (5)$$

Though not reported here, similar results are obtained when the local heat transfer coefficients are linearly integrated over the test section heat transfer surface. The enhancement factor (η) is defined as

$$\eta = \frac{h}{h_0} \quad (6)$$

where subscript h_0 represents the case when the electrode is not charged with the applied voltage. The EHD power consumption is determined by

$$Q_{EHD} = \phi I_e \quad (7)$$

where ϕ and I_e are the applied electric field potential and current, respectively. Finally, the EHD power consumption ratio (α) is defined as

$$\alpha = \frac{Q_{EHD}}{Q} \times 100\% \quad (8)$$

where α quantifies the ratio of electrical power consumed by the electrodes relative to the test section heat transfer rate.

4. Experimental uncertainty analysis

The measurement errors for the condensation experiments are summarized in Table 2. Utilizing the propagation of errors principle, the experimental uncertainty of measuring the averaged heat transfer coefficient (Δh) was estimated to range from ± 1.7 to $\pm 17.3\%$. Among the parameters considered in the analyses, temperature measurements contributed the most to Δh. When the temperature difference ($T_s - T_w$) decreased, Δh became more significant. The lowest ($T_s - T_w$) usually took place at the lowest applied heat flux.

Table 2
Experimental errors in the measurements

Measurement	Error
Pressure (P)	$\pm 0.11\%$ of the reading
Temperature (T)	$\pm 0.1^\circ$C
Applied EHD voltage (ϕ)	$\pm 0.1\%$ of the reading
Applied EHD current (I_e)	$\pm 0.1\%$ of the reading
Heater voltage (V)	$\pm 0.7\%$ of the reading
Heater current (I)	$\pm 0.1\%$ of the reading

5. Results and discussions

5.1. Base case data comparison

Base case (without electrode) external condensation experiments were conducted on a smooth tube in both horizontal and vertical tube orientations. All experiments were performed at a saturation pressure of 551.6 kPa (80 psia). The applied heat flux ranged from 3000 to 15 000 W m^{-2}. The objectives of the base case experiments were first to establish a reference level against which results of the later, EHD-coupled experiments could be compared, and second to verify the validity of the experimental setup and procedure by comparing the results with those available in the literature. As shown in Fig. 4, our data on horizontal condensation agree well with Nusselt's analysis, with a maximum deviation of about $\pm 8\%$.

For the vertical smooth tube experiments, the film Reynolds number ranged from 0 to 300, which indicates a wavy-free laminar to a wavy laminar flow regime. Figure 5 presents our experimental data together with the averaged heat transfer coefficients calculated by the correlations from Nusselt [7], Rohsenow [8] and Kutateladze [9]. It is shown that the experimental results compared very well with those obtained from the correlations. The mean deviations of our data from Kutateladze's correlation, Nusselt's analysis and Rohsenow's analysis were within $\pm 7\%$. The findings verified the reliability and

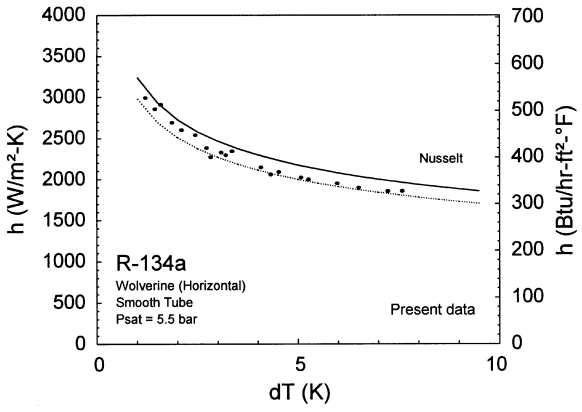

Fig. 4. Base case (w/o electrode) comparison for horizontal smooth tube external condensation experiments.

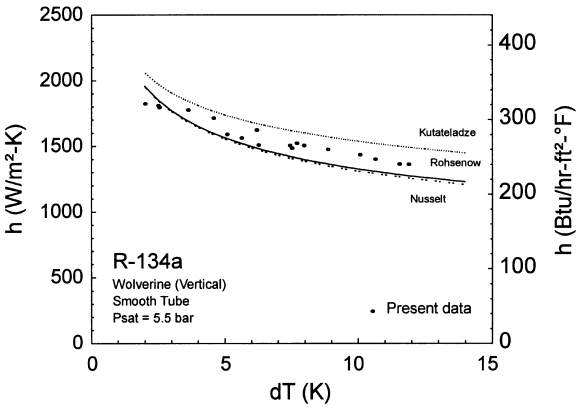

Fig. 5. Base case (w/o electrode) comparison for vertical smooth tube external condensation experiments.

accuracy of the experimental facility and the methodology of testing and data analysis.

5.2. Results of the vertical smooth tube experiments

The effect of EHD on the average heat transfer coefficient (i.e. heat transfer coefficient based on the average temperature) is shown in Fig. 6, where the data were taken at a heat flux of 15 000 W m^{-2} and an electrode gap of 3.2 mm. It is clear that the heat transfer coefficient (h) increases for the most part nearly linear with the applied voltage (ϕ). This finding is quite different from that of the EHD-assisted boiling experiments, where there is an optimum voltage at which the heat transfer coefficient is maximum [10]. In an EHD-enhanced boiling phenomena excessive EHD force can dry out some parts of the heat transfer surface, decreasing the effectiveness of heat transfer. By contrast, for EHD-enhanced condensation, an effective heat transfer enhancement is

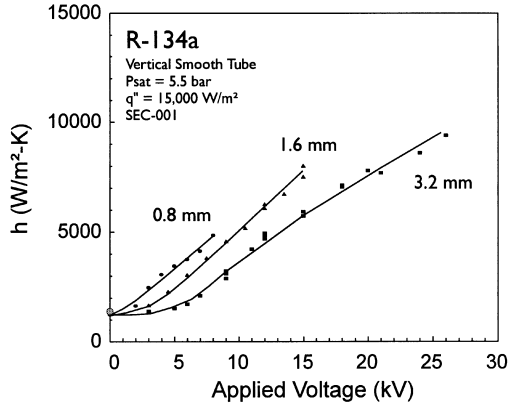

Fig. 6. Effect of applied voltage on h for vertical smooth tube external condensation.

associated with strong EHD body force to remove the condensate from the heat transfer surface, thus reducing the overall thermal resistance and improving the heat transfer coefficient. Accordingly, it is preferable to have a higher applied voltage in an EHD-assisted external condensation, which will provide a stronger EHD-induced force to extract and remove more liquid condensate from the heat transfer surface.

Further analysis of the data in Fig. 6 suggests that for the particular electrode gap tested (3.2 mm), the heat transfer coefficient increases sharply after an applied voltage of about 5 kV. Below this applied voltage, the EHD effect on further improvement of the heat transfer coefficient is minimal. Flow visualization observations also confirmed that the EHD force began to extract the condensate from the tube surface to the electrode at about 5 kV. Consequently, it is concluded that the reduction of film condensate thickness contributes greatly to the heat transfer enhancement in EHD-assisted external condensation.

Once the liquid condensate is extracted from the tube surface to the electrode wires, it is then removed by two means: (1) the centripetal force created while the condensate sweeps along the helical wires and (2) the EHD-induced liquid dispersion occurred on the electrode wire. The former mostly occurs at low applied voltages (<10 kV for the present case with 3.2 mm electrode gap). However, the latter effect becomes more dominant when the applied voltage is higher, allowing a strong electric field intensity on the electrode, thus enabling the dispersion process to take place.

Figure 6 also depicts the maximum heat transfer enhancement obtained in the vertical smooth tube condensation experiments for the range of parameters tested. Up to 620% increase in heat transfer coefficient (which is equivalent to a heat transfer coefficient of 9400 W m^{-2} and an enhancement factor of 7.2) was achieved at an applied voltage of 26 kV. However, despite the large enhancement, a negligible amount of EHD power was required (only 0.06% of the heat transfer rate). Note that the large dot in Fig. 6 represents the heat transfer coefficient obtained when the electrode was removed. It was found that the presence of the electrode itself (without the electric field applied) does not have significant effect on the heat transfer coefficient.

In the present study, optimization of the electrode gap was primarily based on the heat transfer enhancement and the EHD power consumption. Figure 7 shows the heat transfer coefficients as a function of the EHD power consumption ratio for three different electrode gaps at $q = 15\,000$ W m^{-2}. Results indicate that the electrode gap of 3.2 mm is the optimal among the three electrode gaps tested. To yield a given heat transfer coefficient, a larger electrode gap requires a smaller amount of EHD power. Similar results are obtained at a lower heat flux of 8000 W m^{-2}, as shown in Fig. 8. In addition, both

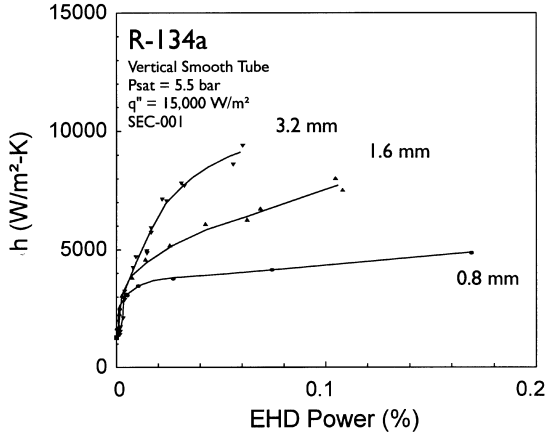

Fig. 7. EHD power consumption ratios vs h for the three electrode gaps tested ($q'' = 15\,000$ W m^{-2}).

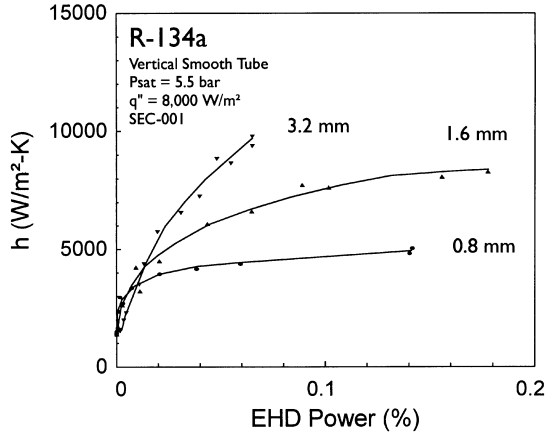

Fig. 8. EHD power consumption ratios vs h for the three electrode gaps tested ($q'' = 8000$ W m^{-2}).

figures suggest that a larger electrode gap yields a higher maximum heat transfer coefficient (h_{max}) and a higher corresponding enhancement factor (η_{max}). Both h_{max} and η_{max} decrease by almost 47% when the electrode gap is reduced from 3.2 to 0.8 mm. Although the use of a smaller electrode gap will decrease the maximum enhancement, a smaller gap requires a much lower applied EHD voltage.

For conventional (non-EHD) external condensation on a vertical smooth tube/plate, an increase in heat flux in general decreases the heat transfer coefficient, due to the increased condensate film thickness, leading to a higher thermal resistance for heat transfer. This trend is evident in Fig. 9 where the heat transfer coefficient as a function of heat flux is depicted for three applied voltages, with an electrode gap of 1.6 mm. All three curves have the same downward trend with increasing heat flux. Hence, one may conclude that, similar to the conventional case, in EHD-enhanced external condensation, the mean film thickness increases with heat flux.

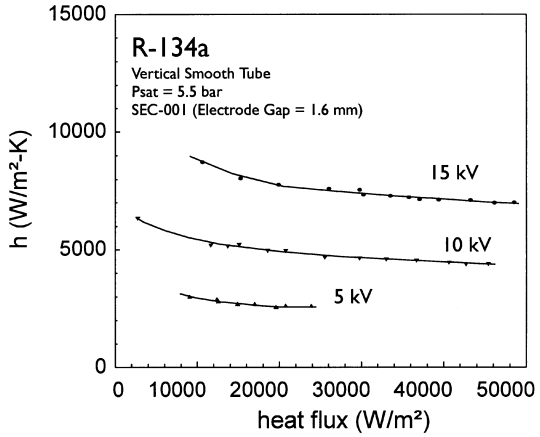

Fig. 9. Effect of heat flux on h in EHD-assisted vertical smooth tube external condensation.

When heat flux increases from 8000 to 15 000 W m^{-2}, the maximum enhancement factor increases from 6.9 to 7.2. The finding suggests that liquid condensate is removed more effectively by EHD force at a higher heat flux. The thicker and less stable condensate film occurring at high heat flux may help for promoting liquid extraction. The EHD power consumption (Q_{EHD}) is also affected by the heat flux. As heat flux increases from 8000 to 15 000 W m^{-2}, Q_{EHD} increases from 0.062 to 0.109 W, though it remains negligible for the range of parameters tested. At a higher heat flux, more liquid condensate is extracted by the electrode. Since liquid is more conductive than vapor, the EHD current increases, leading to the higher power consumption.

5.3. Results of the horizontal smooth tube experiments

Figure 10 depicts the EHD effect on heat transfer coefficient for external condensation on a horizontal smooth tube at a heat flux of 15 000 W m^{-2} and for three different electrode gaps. As is seen in Fig. 10, for all the three cases, the heat transfer coefficient is proportional to the applied voltage, consistent with results for the vertical case (Fig. 7). For all cases, the upper limit in the applied voltage is bounded by the breakdown voltage of the working fluid. Figure 11 again shows similar results obtained with the same electrode gaps but at a lower heat flux of 8000 W m^{-2}.

Attention is next drawn to the case when the heat flux is 15 000 W m^{-2} and the electrode gap is 3.2 mm. The heat transfer enhancement becomes significant when the applied voltage reaches beyond $\sim$8 kV. A similar trend was observed for the vertical case (Fig. 6), but at a lower corresponding voltage $\sim$5 kV. It is suggested that the

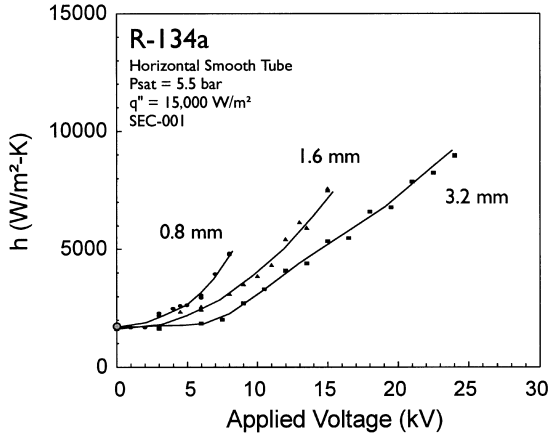

Fig. 10. Heat transfer enhancements obtained with the three electrode gaps tested at $q'' = 15\,000$ W m^{-2}.

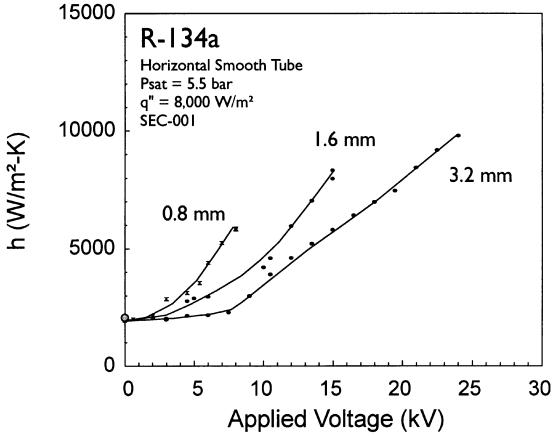

Fig. 11. Heat transfer enhancements obtained with the three electrode gaps tested at $q'' = 8000$ W m^{-2}.

thinner film thickness in horizontal condensation requires a higher electric field intensity, to cause sufficient interfacial instability of the extraction to take place. However, in the vertical condensation, the wavy nature of the condensate film contributes to an unstable interface, causing the liquid extraction process to start sooner. Among the three electrode gaps tested, it is found that the 3.2 mm is the optimum electrode gap for horizontal orientation. This is consistent with the finding for the vertical case, where the 3.2 mm gap yielded higher enhancements and with less EHD power consumption than the other two electrode gaps.

At the higher heat flux (15 000 W m^{-2}), a maximum heat transfer coefficient (h_{max}) of 9000 W m^{-2} K^{-1} (which is equivalent to an enhancement factor of 5.5) is obtained at $\phi = 24$ kV with a 3.2 mm electrode gap. However, at the lower heat flux (8000 W m^{-2}), the enhancement factor reduces to 4.9 while the maximum heat transfer coefficient is 9800 W m^{-2}. The combined findings from both vertical and horizontal condensations suggest that EHD enhancements are more pronounced at higher heat fluxes. Results also show an increase in the EHD power consumption at a higher heat flux (0.139 W at 8000 W m^{-2} and 0.168 W at 15 000 W m^{-2}), though in all cases, the power consumption relative to the heat exchange rate in the test section is negligible.

Finally, for comparison purposes, results of the vertical and horizontal orientation for the base case (no EHD) and the maximum enhancement case are brought together in Table 3. It is seen that in the absence of the EHD effect, the horizontal condensation heat transfer coefficients are higher than those of the vertical condensation (differences of 30 and 21% for heat flux of 8000 and 15 000 W m^{-2}, respectively). However, when the EHD field is applied, the difference between horizontal and vertical condensation, for the most part, diminishes. This is an interesting finding which suggests that in EHD-assisted condensation, the induced EHD force plays a much more dominant role than the gravitational force, thus minimizing the test section orientation effect on the heat transfer coefficients.

6. Conclusions

The feasibility of implementing the EHD technique to improve external condensation heat transfer was demonstrated in the present work. It is concluded that the EHD enhancement technique responds remarkably well for external condensation applications. In the present experiments up to 7.2 fold enhancement in heat transfer coefficient with an EHD power consumption of only 0.06% was reported.

The heat transfer enhancement mechanism involves an effective removal process of liquid condensate from the tube surface, minimizing the film thickness by utilizing the EHD-induced forces. However, this requires a careful design of the electrode to yield maximum enhancement at minimum power consumptions. Among the electrode gaps tested, the 3.2 mm gap yielded the highest heat transfer enhancement and required the least amount of electrical power to the electrodes.

When the EHD field is applied, the significant difference that otherwise exists between heat transfer coefficients of the horizontal and vertical condensation diminishes almost entirely. Therefore, an EHD-assisted condenser is insensitive to the orientation providing further in-space utilization flexibility.

The effect of heat flux on EHD-assisted external condensation was also investigated. For the range of parameters tested, it is found that the maximum heat transfer coefficient shows a decreasing trend with increasing heat flux in all cases. However, the maximum enhancement

Table 3
Differences in h between vertical and horizontal condensation

q [W m^{-2}]	Horizontal without EHD [W m^{-2} K^{-1}]	Vertical without EHD [W m^{-2} K^{-1}]	% diff	Horizontal with EHD [W m^{-2} K^{-1}]	Vertical with EHD [W m^{-2} K^{-1}]	% diff
8 000	2000	1400	30%	9800	9600	2%
15 000	1650	1300	21%	9000	9400	4%

factor increases as the heat flux increases. It is concluded that the liquid extraction process is more effective at a higher heat flux, where the film in general is thicker and the vapor–liquid interface becomes less stable. This finding is in contrast to what was found in EHD-enhanced pool boiling, where the maximum heat transfer coefficient is in most cases higher at a higher heat flux and the enhancement factor is higher at a lower heat flux level. In general, the EHD power consumption increases with increasing heat flux, however, it remains negligible for all cases when compared to the test section heat transfer rate.

References

[1] A.B. Didkovsky, M.K. Bologa, Vapor film condensation heat transfer and hydrodynamics under the influence of an electric field, International Journal of Heat and Mass Transfer 24 (1981) 811–819.
[2] A. Yabe, T. Taketani, K. Kikuchi, Y. Mori, K. Hijikata, Augmentation of condensation heat transfer around vertical cooled tubes provided with helical wire electrodes by applying nonuniform electric fields, International Heat Transfer Science and Technology (1987) 812–819.
[3] Sunada, Kazumi, A. Yabe, T. Taketani, Y. Yoshizawa, Experimental study of EHD pseudo-dropwise condensation, Proceedings of ASME/JSME Thermal Engineering 3 (1991) 47–53.
[4] K. Yamashita, A. Yabe, Electrohydrodynamic enhancement of falling film evaporation heat transfer and its long term effects on heat exchangers, Journal of Heat Transfer 119 (1997) 339–347.
[5] K. Yamashita, M. Kumagai, S. Sekita, Heat transfer characteristics on an EHD condenser. ASME/JSME Thermal Engineering Proceedings 3 (1991) 61–67.
[6] K. Cheung, Electrohydrodynamic (EHD) Enhancement of shell-side phase change heat transfer of alternate refrigerants, Ph.D dissertation, University of Maryland, MD, U.S.A., 1996.
[7] W. Nusselt, Die Oberflachenkondensation des Wasser damfes, Z. Vereins deutscher Ininuere 60 (1916) 541–575.
[8] M.W. Rohsenow, Heat transfer and temperature distribution in laminar film condensation, Transactions of the American Society of Mechanical Engineering 78 (1956) 1645–1651.
[9] S.S. Kutateladze, Fundamentals of Heat Transfer, Academic Press, New York, 1963.
[10] K.H. Cheung, M.M. Ohadi, S. Dessiatoun, Enhanced boiling coefficients and visualization of R-134a over enhanced tubes, Journal of Heat Transfer 119 (1997) 332–338.